Preliminary Design of the NISAR L-Band Feed Antenna Tiles

Paolo Focardi and Paula R. Brown
Jet Propulsion Laboratory, California Institute of Technology,
4800 Oak Grove Dr., Pasadena, CA 91109
Paolo.Focardi@jpl.nasa.gov, Paula.Brown@jpl.nasa.gov

***Abstract*—Being developed in partnership between NASA and the Indian Space Research Organisation (ISRO), the NASA-ISRO Synthetic Aperture Radar (NISAR) satellite is planned to launch in late 2020. NISAR will measure many aspects of how Earth is changing with unprecedented accuracy on a global scale from a Low Earth Orbit (LEO) platform. With a 12m deployable mesh reflector, NISAR will feature one of the largest deployable mesh reflector ever launched for a scientific mission. Two large planar phased arrays will feed the reflector, one that will operate at L-Band and be developed by the Jet Propulsion Laboratory (JPL), and an S-band array that will be developed at the ISRO Space Application Centre (SAC). This paper describes the preliminary design of the L-Band feed array.**

Keywords—phased array; planar array; deployable mesh reflector; patch antenna; metal patch antenna.

I. Introduction

The basic operational principle of the NISAR radar with its SweepSAR mode is illustrated in Fig. 1. The L-Band feed will be an array of 2x12 patches, organized in pairs, located near the spacecraft bus. During transmit operation, all the patch elements are fed, under-illuminating the reflector in elevation. Consequently, the 12m reflector generates a beam that is wide in elevation and covers the entire radar swath on the ground. During receive operation, the patch pairs are processed in subsets using digital beam-forming. By "sweeping" through digital beam-formed combinations of the 12 patch pairs, the radar captures data from a wide swath with high resolution [1]. Once the radar data are processed, NISAR will provide science products ranging from biomass disturbance, to ice velocity and thickness, to surface deformation due to earthquakes, other natural disasters, or global effects such as climate change. This paper describes the preliminary design of the NISAR L-Band feed array. Section II covers the basic geometry of the array including details of the feeding network, the stacked patch arrangement, the feeding mechanism, and the radome. Section III presents the calculated return loss performance of the array while Section IV presents some preliminary measurements. The secondary antenna performance is not included here.

II. Geometry of the L-Band Feed Array

The L-Band feed array consists of six tiles, with two patch pairs per tile. Each patch pair is required to provide horizontal, vertical, and circular polarization. Therefore the feeding network needs to accommodate all of the above possibilities in a compact package.

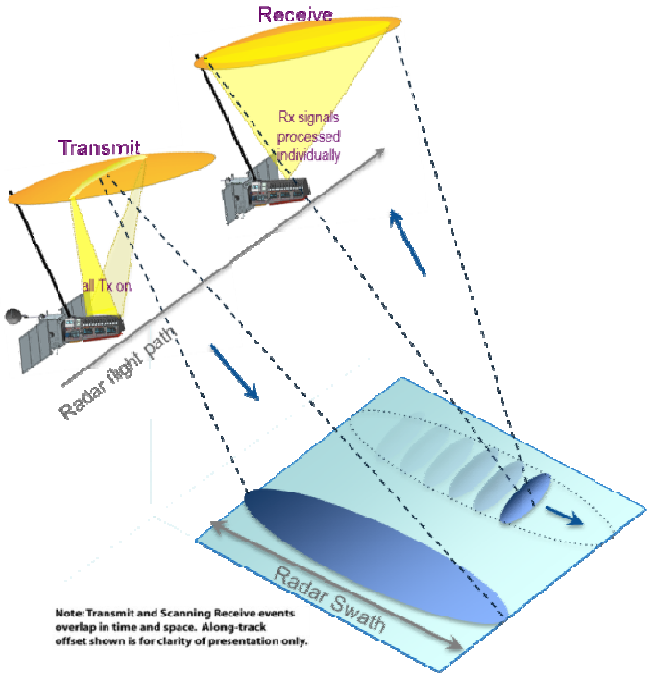

Fig. 1, Sweep SAR technique will allow global coverage.

Differential probe feeds are used to minimize cross-polarization and to maintain a high degree of symmetry along the array. Since each patch must operate in two linear polarizations, a total of four probes are needed per patch. A stripline feeding network made in Rogers 6002 provides the proper power splitting and phasing to feed the patch pairs. The patches, organized in a stacked patch configuration to widen the bandwidth, are supported by the feed probes plus a center post for structural rigidity. There is no dielectric under the patches. The lower patch is capacitively fed, which enables proper tuning of the patch. The top patch is directly soldered to the probes. A center post adds structural rigidity, and has the side benefit of naturally rejecting the second harmonic that is generated by the Transmit/Receive Modules (TRMs). Fig. 2 shows the main body of the Radar Instrument Structure (RIS), including the top deck with both the L-Band and the S-Band feed arrays. The L-Band and S-Band TRMs are located both inside and outside the RIS. Each L-Band tile is covered by a radome. The radome shell is made of a 1mm thick Astroquartz layer and is painted for thermal control and protection from atomic oxygen corrosion. Inside the radome shell, a foam layer

with cut-outs for the patches provides additional thermal insulation.

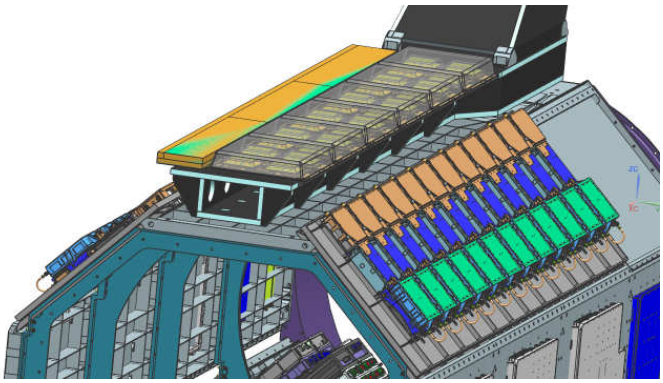

Fig. 2, The Radar Instrument Structure (RIS) with the six L-Band Tiles on the top deck. The radomes of the L-Band tiles in this view are semi-transparent. Also visible is the base of the reflector boom at one end of the array. The TRMs are located on both sides of the RIS.

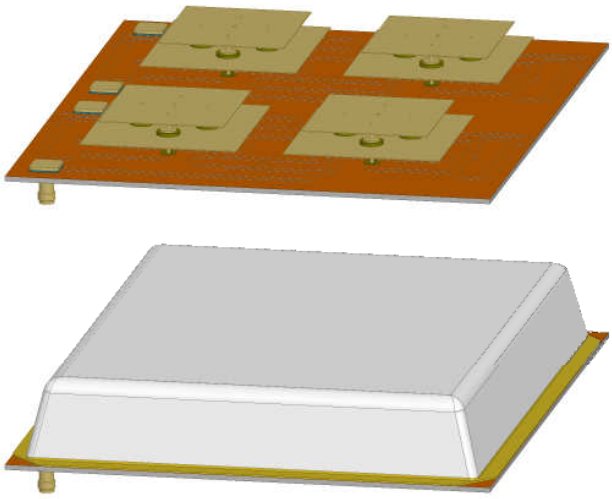

Fig. 3, A L-Band tile with (top) and without (bottom) radome

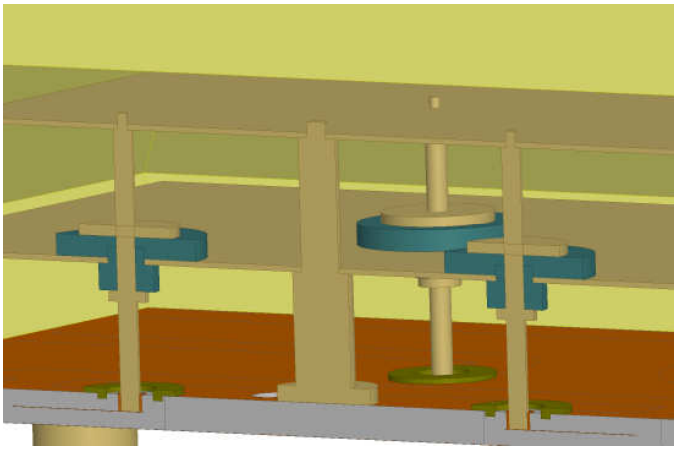

Fig. 4, Detail of the patch feeding mechanism.

Fig. 3 shows a single L-Band tile with and without the radome. Fig. 4 shows the patch feeding mechanism in more detail. The four feed probes in each stacked patch are soldered to the feed network board. They then support a dielectric bushing which supports the lower patch. An upper dielectric bushing in combination with a metal washer is used to capacitively couple power to the lower patch. The upper patch is directly soldered to the four probes and the center post. Since each patch pair is fed 300W of peak power when operated in circular polarization, power breakdown was a concern during the design. Additional dielectric washers at the base of the probes were used to prevent multipactor breakdown at the feed network board interface by creating a dielectric barrier between the feed probes and the ground plane. Care was also used to minimize the potential for passive intermodulation products at metal-to-metal interfaces.

III. Calculated Performance

The six-tile L-Band feed array, including the feed network, was simulated in HFSS™. Fig. 5 shows the calculated return loss at the input connector ports of the array for both horizontal and vertical polarizations. While the requirement is -15dB, all ports currently show a return loss better than -20dB except for the first patch pair in vertical polarization on one end of the array, therefore providing adequate margin to accommodate performance variations over expected manufacturing tolerances and the operating temperature range.

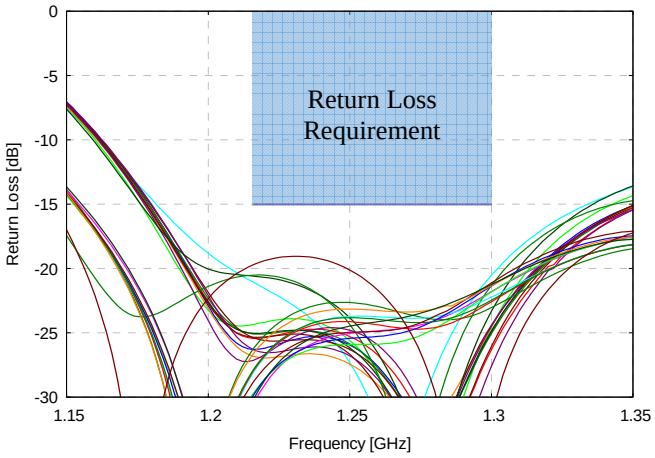

Fig. 5, Calculated return loss at all ports during transmit for both polarizations.

IV. Preliminary Measurements

In order to verify the RF design, two prototype tiles were fabricated and tested, including a third board for the feeding network alone. This latter board was “connectorized” also on the top side where the patch probes are supposed to be attached. This way we could measure exactly the insertion loss of the board itself. Fig. 6 shows an example of the measured versus calculated performance obtained with our RF design of the feeding network. Each of those curves represent the pertinent S-parameter between a V-pol input port and the corresponding four ports where one patch would be located in

the complete design. As can be observed from Fig. 6 the agreement is quite good.

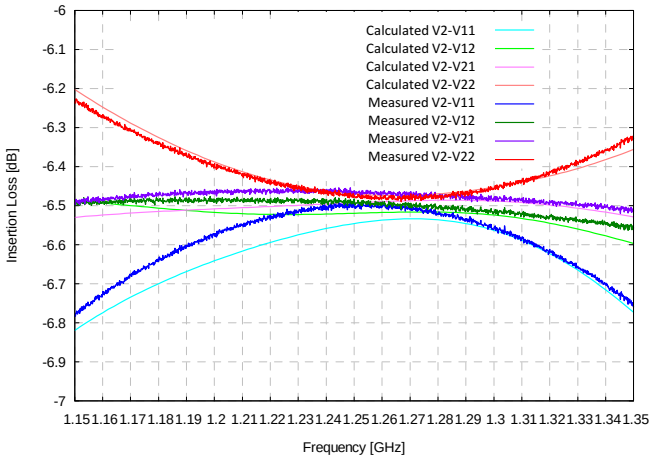

Fig. 6, Calculated Vs. Measured S_{21} parameters for a V-pol port in the feeding network test board.

Fig. 6 also shows about 0.5 dB of insertion loss for V-Pol at center frequency which is reasonable for this kind of feeding network. The return loss of the complete tile was also measured. The first measurements were not in good agreement with our calculations unfortunately. Then we realized that the model and the actual geometry were not exactly the same. In particular, as shown in Fig. 4, the lower patch is capacitively coupled to the probes. The dielectric bushings are therefore responsible for the RF tuning of this interface, and in the final revision some small venting holes were added to the design of these parts. These small holes were not implemented in the model, but they actually changed the equivalent dielectric constant of the tuning feature. The dielectric constant itself was also close to the nominal value but not quite the same. Once both of these small discrepancies were included in our tile model, measured and calculated return loss were again in good agreement and most important we met our requirement.

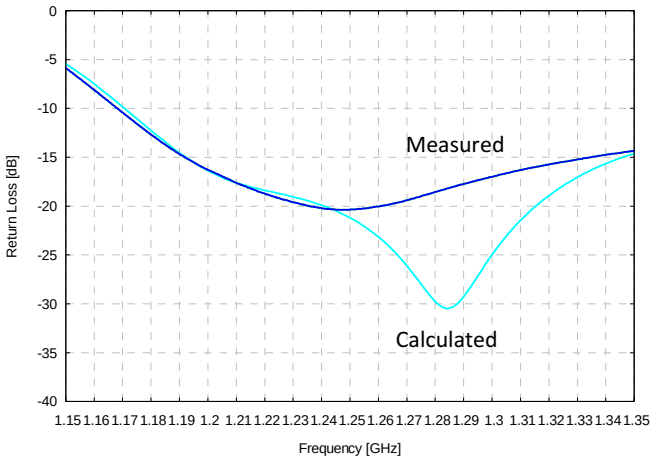

Fig. 7, Calculated Vs. Measured return loss for a H-pol port of the complete tiles after being retuned.

The change in effective dielectric constant also needed to be compensated with a small change in the capacitor size (the metal washer above the bushing in Fig. 4). After these changes were implemented measured and calculated data agreed again to a satisfactory level. Also, the model shows a dip in return loss around 1.28 GHz which is not present in the measurements. Clearly there is still some small detail missing for a perfect match but the agreement was considered good enough. Directivity, gain and overall insertion loss were also measured along with radiation patterns. All measured values were well within the expected ranges predicted by the RF model and showed similar trends in frequency.

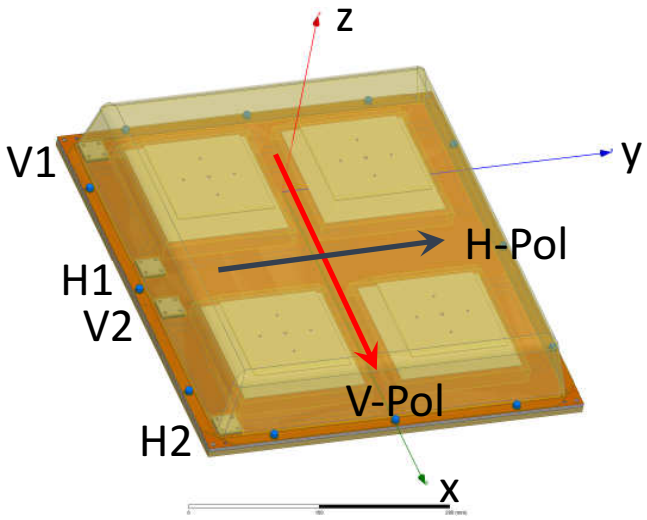

Fig. 8, Tile model showing the orientation of the two polarizations and the corresponding input ports, along with the associated reference system.

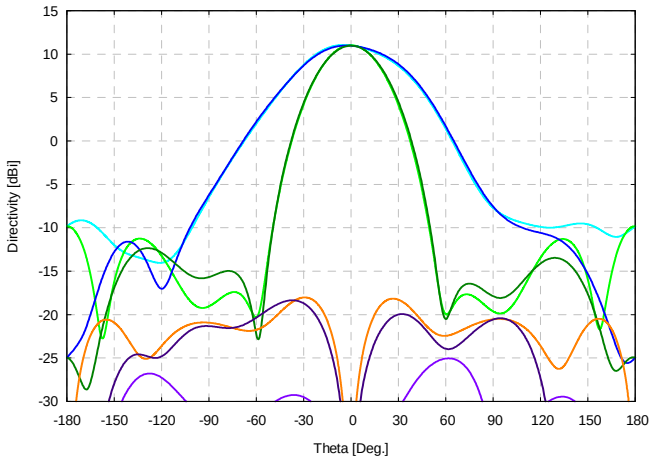

Fig. 9, Radiation pattern on the two principal cuts for port H1 in Fig. 8. Blue curves are for the Elevation cut (Phi = 0°), green curves are for the Azimuth cut (Phi = 90°). Lighter colors are calculated, darker colors are measured.

Fig. 9 shows an example of measured and calculated radiation patterns for one of the H1 port. The measurements were performed in an NSI spherical near field range in Torrance, CA. As we approach the back lobe in the data, the measured data progressively grow further apart from the

calculations. This is mostly due to the presence of absorber behind the antenna.

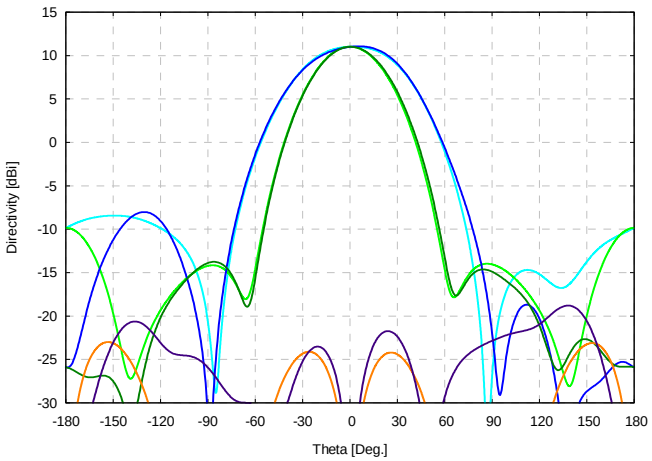

Fig. 10, Radiation pattern on the two principal cuts for port V1 in Fig. 8. Blue curves are for the Elevation cut (Phi = 0°), green curves are for the Azimuth cut (Phi = 90°). Lighter colors are calculated, darker colors are measured.

Fig 10, shows the radiation pattern data for a V-Pol port. Similar considerations apply to this figure; the agreement is very good until we reach the back lobe were the absorber tends to reduce the measured levels. Cx-Pol level are also well within our requirements and in good agreement with the predicted values (orange lines in Fig. 9 and Fig. 10). It is also important to note that the subtended angle of the reflector is about ±35° and in that range the model is predicting the performance of the radiation pattern very well. These prototypes were also tested over temperature and cycled over the full extent of our required proto-flight temperatures which covers almost a 200°C span. Performance mostly didn't change after thermal cycling but we noticed a slight improvement in the overall insertion loss vs. frequency plots. This, we believe, was due to some residual mechanical stress left over in the tiles after the assembly. Thermal cycling relieved the residual stress and made the overall tile perform a little more efficiently. Changes of almost 0.1 dB were observed.

V. Conclusions

A preliminary design of the NISAR L-Band feed antenna tiles has been completed and two prototype tiles have been fabricated and tested with good agreement with predicted performance. A compact feeding network capable of providing H-Pol, V-Pol and Circular Polarization was designed and tested with very good results. A patch feeding mechanism that provides mitigation features against power breakdown was also developed and promises to provide at least 10 dB of margin over the expected power levels. Overall a compact and lightweight design for the feed tiles was finalized and we are now in the process of building a full set of EM tiles which will be used to test the full array.

Acknowledgment

The research was carried out at the Jet Propulsion Laboratory, California Institute of Technology, under a contract with the National Aeronautics and Space Administration. © 2016 California Institute of Technology. Government sponsorship acknowledged.

References

[1] A. Freeman, G. Krieger, P. Rosen, M. Younis, W. Johnson, S. Huber, R. Jordan, A. Moreira, "SweepSAR: Beam-forming on receive using a reflector-phased array feed combination for spaceborne SAR," 2009 IEEE Radar Conference, pp.1-9, 4-8 May 2009.